Available online at www.sciencedirect.com
SCIENCE DIRECT
Journal of Photochemistry and Photobiology A: Chemistry 178 (2006) 130–139
Journal of Photochemistry and Photobiology A:Chemistry
www.elsevier.com/locate/jphotochem

# Excitation energy migration in a dodecameric porphyrin box

In-Wook Hwang [a,1], Zin Seok Yoon [a], Jiwon Kim [b], Taisuke Kamada [c], Tae Kyu Ahn [a], Naoki Aratani [c], Atsuhiro Osuka [c,*], Dongho Kim [a,*]

[a] *Center for Ultrafast Optical Characteristics Control and Department of Chemistry, Yonsei University, Seoul 120-749, Republic of Korea*
[b] *Department of Chemistry, Korean Advanced Institute of Science and Technology, Daejeon 305-700, Republic of Korea*
[c] *Department of Chemistry, Graduate School of Science, Kyoto University, and CREST (Core Research for Evolutional Science and Technology) of Japan Science and Technology Agency, Kyoto 606-8502, Japan*

Available online 28 November 2005

Dedicated to Professor I. Yamazaki of Hokkaido University.

**Abstract**

The excitation energy hopping (EEH) in a dodecameric porphyrin box (**TB2**) prepared by self-assembly of four *meso–meso* linked zinc(II) triporphyrin (**T2**)s is explored by picosecond fluorescence and femtosecond transient absorption (TA) spectroscopy. The exciton–exciton annihilation and anisotropy depolarization observed in both fluorescence and TA provide a consistent EEH rate, i.e. $300 \pm 20\,ps^{-1}$, assuming Förster energy hopping among four **T2** units in **TB2**. The observed energy hopping time $300 \pm 20\,ps^{-1}$ is slower than the previous $98 \pm 3\,ps^{-1}$ of **B2** (an octameric porphyrin box), even though the size of hopping unit is larger in **TB2**.


*Keywords:* Self-assembled porphyrin array; Exciton coupling; Excitation energy hopping (EEH); Transient absorption anisotropy (TAA); Exciton–exciton annihilation; Coupling energy matrix

## 1. Introduction

The mimicry of natural light harvesting complexes has continuously been attempted by various types of porphyrin or related pigment arrays with the goal of applying these arrays to artificial light harvesting apparatus and molecular photonic devices [1–9]. In view of synthesis, covalent approach encounters with various difficulties as the array becomes complicate. In contrast, supramolecular chemistry using a strategy of non-covalent self-assembly has recently been a judicious choice to prepare multi-porphyrin arrays [10]. The coordination between zinc(II) porphyrin and pyridine is particularly useful, because of its easy manipulation, relatively large association, and favorable tendency not to deteriorate the excited-state photophysics of constituent porphyrin moiety [11]. Interesting examples so far reported include oligomeric conjugated porphyrin ladders developed by Anderson et al. that exhibit very large two-photon absorption cross-section [12], energy and electron transfer assemblies reported by Hunter et al. [13], and giant porphyrin arrays and large porphyrin wheels as a model of light harvesting antenna reported by Kobuke et al., where an imidazoyl substituent is used instead of a pyridyl substituent [14].

In the present study, we have prepared a three-dimensional dodecameric porphyrin box (**TB2**) with an aid of self-assembly of pyridine-appended-orthogonally-linked zinc(II) triporphyrin (**T2**)s (Scheme 1). Four **T2** molecules assemble into **TB2** in non-coordinating $CHCl_3$ by means of axial coordination between zinc(II) central metal ions of **T2** and peripheral pyridyl units of another neighboring **T2**. The structure of **TB2** was previously characterized by $^1H$ NMR, GPC (gel permeation chromatography), and absorption/fluorescence spectroscopy, where **TB2** revealed a large association constant (at least $10^{24}\,M^{-3}$) that was estimated by the concentration dependence on the absorption/fluorescence spectra [15]. The molecular components of **TB2** are quite attractive in view of mutual perpendicular geometry. Because the porphyrin units are strongly coupled

* Corresponding authors.
*E-mail addresses:* osuka@kuchem.kyoto-u.ac.jp (A. Osuka), dongho@yonsei.ac.kr (D. Kim).
[1] Current address: Center for Polymers and Organic Solids, University of California at Santa Barbara, Santa Barbara, CA 93106, United States.

1010-6030/$ – see front matter © 2005 Elsevier B.V. All rights reserved.
doi:10.1016/j.jphotochem.2005.10.029

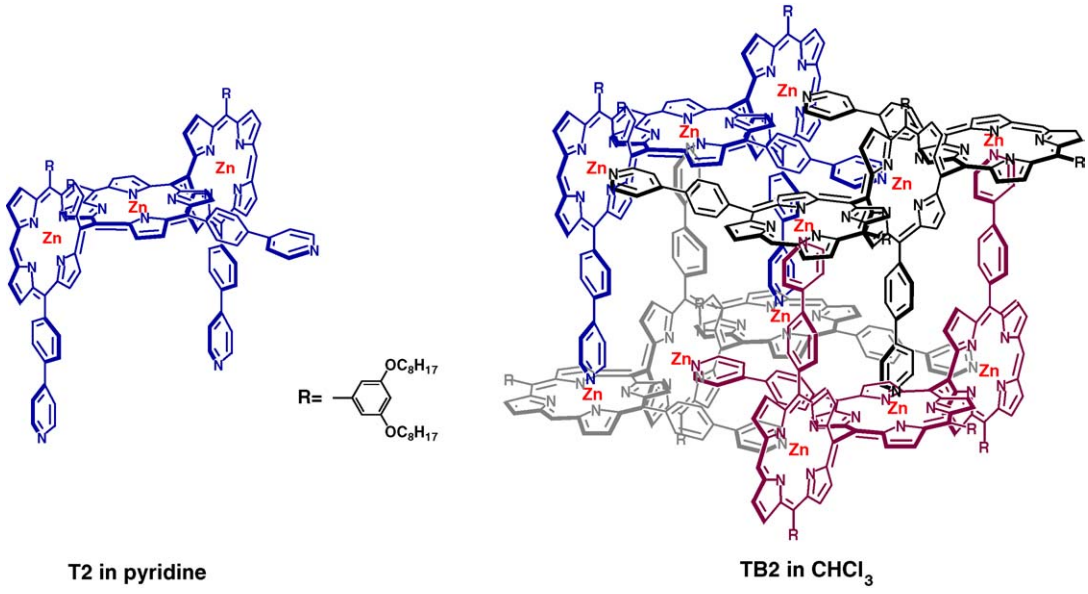


Scheme 1. Structures of **T2** and **TB2**. R = 3,5-dioctyloxyphenyl.

mainly through Coulombic interaction but not π-conjugated, **TB2** would be a good candidate for three-dimensional light-harvesting antenna.

Here, we report the excitation energy hopping (EEH) occurring in **TB2**, which is clarified by time-resolved fluorescence and transient absorption (TA) spectroscopy. While the steady-state absorption/fluorescence measurements provide relevant information about excitonic dipole coupling among the porphyrin units, the time-resolved spectroscopic measurements can quantify the EEH rate. The anisotropy depolarization observed in both time-resolved fluorescence and TA is useful, because the initial localization of excitations in weakly coupled multichromophores leads to fast anisotropy depolarization as the excitation energy is transferred. In addition, the exciton–exciton annihilation which can be observed in both time-resolved fluorescence and TA is also well associated with the EEH rate, because this process is conceived as an incoherent energy hopping from the excited donor to the proximal excited acceptor [9,14,15]. With the aids of these two observables, we are able to quantify the EEH rate over **TB2**. Throughout the measurement, **T2** dissolved in strongly coordinating pyridine has been used as reference for **TB2** dissolved in $CHCl_3$, to elucidate the unique property of **TB2**.

## 2. Experimental section

### 2.1. Steady-state spectra

The samples were prepared in approximately micromolar concentrations in $CHCl_3$ and pyridine, respectively. The solvents (~99.9% purity) were purchased from Merck Chemical Co. (HPLC grade). Absorption spectra were obtained with a Shimadzu model 1601 UV spectrophotometer, and steady-state fluorescence and fluorescence excitation spectra were measured by a Hitachi model F-2500 fluorescence spectrophotometer at room temperature. The excitation anisotropy spectra were obtained by changing the fluorescence detection polarization either parallel or perpendicular to the polarization of the excitation light. The excitation anisotropy spectra then were calculated [6,15]. The fluorescence quantum-yields were obtained in comparison with $\Phi_F = 0.03$ of zinc(II) tetraphenylporphyrin in toluene at room temperature.

### 2.2. Fluorescence and fluorescence-anisotropy decays

A picosecond time-correlated single photon counting (TCSPC) system was used for the fluorescence and fluorescence anisotropy decay measurements [9,14,15]. Especially, the excitation power dependence on the fluorescence decay was explored in this study, by adjusting the excitation laser fluence with an aid of variable neutral-density filter. In the measurement, the slit width in front of monochromator and photomultiplier tube were fixed to eliminate the geometrical artifacts.

### 2.3. Transient absorption and transient absorption anisotropy decay

A dual-beam femtosecond time-resolved transient absorption spectrometer with an IR-OPA (infra-red optical parametric amplifier) as pump pulses and white light continuum as probe pulses was employed for TA and transient absorption anisotropy (TAA) measurements. The system has also been described in previous reports [9,14,15].

## 3. Results

### 3.1. Construction of *T2* and *TB2*

The synthetic route to **T2** was previously reported [15]. The summary is as follows. The Ag(I)-promoted coupling reaction

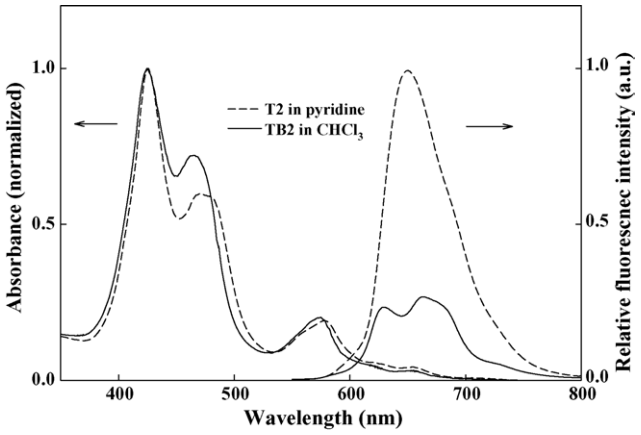


Fig. 1. Steady-state absorption (left) and fluorescence (right) spectra of **T2** in pyridine and **TB2** in $CHCl_3$. The fluorescence spectra were obtained with the excitation wavelength 420 nm, on which the excitation wavelength dependence was negligible.

of a pyridyl-appended zinc(II) porphyrin monomer, i.e., zinc(II) 5-(3,5-dioctyloxyphenyl)-15-[4-(4-pyridyl)phenyl]porphyrin gave *meso–meso* coupled diporphyrin **D2** and triporphyrin **T2** along with higher oligomers. Since the separation of these oligomers was practically impossible due to serious self-aggregation, these zinc(II) complexes were once demetallated to their corresponding free-base porphyrin oligomers, which were separated over preparative GPC to provide diporphyrin **D2H** and triporphyrin **T2H** in 32 and 14%, respectively. The free-base triporphyrin **T2H** was separated into two diastereoisomers **T2H-a** (fast eluting, 4%) and **T2H-b** (slow eluting, 10%) through a silica gel column. Zinc(II) insertion into **T2H-a** led to formation of insoluble and intractable polymeric material, while **T2H-b** gave a soluble discrete zinc complex that displayed a clear $^1$H NMR spectrum. The $H^{\alpha}$ and $H^{\beta}$ protons in the pyridyl substituents are observed at 2.82, 3.32, 6.09, and 6.28 ppm, hence suggesting the box formation [15]. These results are based on the stereochemistry of **T2H**. **T2H-a** and **T2H-b** have been assigned respectively as *dl*-**T2H** and *meso*-**T2H** isomers.

### 3.2. Steady-state absorption, fluorescence, and fluorescence excitation anisotropy

Fig. 1 shows the absorption and fluorescence spectra of **T2** in pyridine and **TB2** in $CHCl_3$, respectively. The peak positions are summarized in Table 1. The absorption spectrum of **T2** is different from that of non-pyridine-appended and *meso–meso* linked zinc(II) triporphyrin (**Z3**). **Z3** exhibits two Soret bands [6] ($\lambda_{max}$ = 414 and 473 nm in $CHCl_3$) that reflect exciton coupling among three orthogonally-linked zinc(II) porphyrin monomers, whereas **T2** shows three Soret bands ($\lambda_{max}$ = 425, 469, and 480 nm), plausibly indicating wide distribution in dihedral angle between the porphyrin units. The bulky (4-pyridyl)phenyl units asymmetrically substituted to each porphyrin are likely to perturb the orthogonal geometry (90° dihedral angle) between the porphyrin units, resulting in an electronic interaction. This was indeed confirmed by the examination of a series of permanently distorted 1,ω-dioxymethylene-strapped *meso–meso* linked zinc(II) diporphyrins with dihedral angle less than 90° that led to broad Soret bands including charge transfer bands [7]. In contrast to **T2**, **TB2** shows two Soret bands that are well split at 425 and 465 nm, with a smaller splitting energy than those of **T2** and **Z3**. The well split Soret bands indicate the rigidification of perpendicular geometry of **TB2** that is driven by 12 zinc(II)-pyridine cooperative coordinations. The small Soret band splitting energy attributed to blue shift in the low-energy Soret band also reflects three-dimensional exciton coupling scheme among 12 porphyrin units, which encourages Förster-type incoherent energy hopping over **TB2** (vide infra).

The fluorescence spectra indicate the same molecular geometries as described in the absorption spectra. The broad fluorescence spectrum occurring in **T2** is interpreted in terms of wide distribution in the dihedral angle between porphyrin units, because changes in the dihedral angle influence the electronic interaction between the porphyrin units, resulting in a different spectral character from two split fluorescence bands [6] ($\lambda_{max}$ = 600 and 650 nm in toluene) occurred in zinc(II) porphyrin monomer. In contrast to the broad fluorescence spectrum of **T2**, the fluorescence spectrum of **TB2** clearly shows vibronic bands ($\lambda_{max}$ = 628, 663, 680 and 725 nm), indicating smaller electronic interaction between the porphyrin units, which is brought about by fixation of its perpendicular conformation upon the box formation. This characteristic fluorescence spectrum is rather concentration independent up to $1.0 \times 10^{-8}$ M, from which the association constant of **TB2** has been estimated to be at least $10^{24}$ $M^{-3}$. In terms of fluorescence quantum-yield, **TB2** shows six times smaller value than that of **T2**, exhibiting additional deactivation channels in the $S_1$-state (Table 1).

The steady-state fluorescence excitation anisotropy spectra are comparatively measured for **T2** and **TB2** (Fig. 2). The polarization anisotropy measurement is informative for the excitation energy migration, because the energy migration between the same molecular units with different orientations creates a

Table 1
Band maxima in absorption and fluorescence spectra of **T2** and **TB2**

| Sample | Solvent | Absorption (nm) | | | Fluorescence (nm)[a] | |
|---|---|---|---|---|---|---|
| | | Soret (high) | Soret (low) | *Q* | *Q* | $\Phi_F$[b] |
| **T2** | Pyridine | 425 | 469, 480 | 577, 624, 657 | 650 | 0.06 |
| **TB2** | $CHCl_3$ | 425 | 465 | 575, 622, 657 | 628, 663, 680, 725 | 0.01 |

[a] The excitation wavelength 420 nm was used.
[b] The fluorescence quantum-yield $\Phi_F$ was obtained by a relative method, using zinc(II) tetraphenylporphyrin that had a fluorescence quantum-yield of 0.03 in toluene at room temperature.

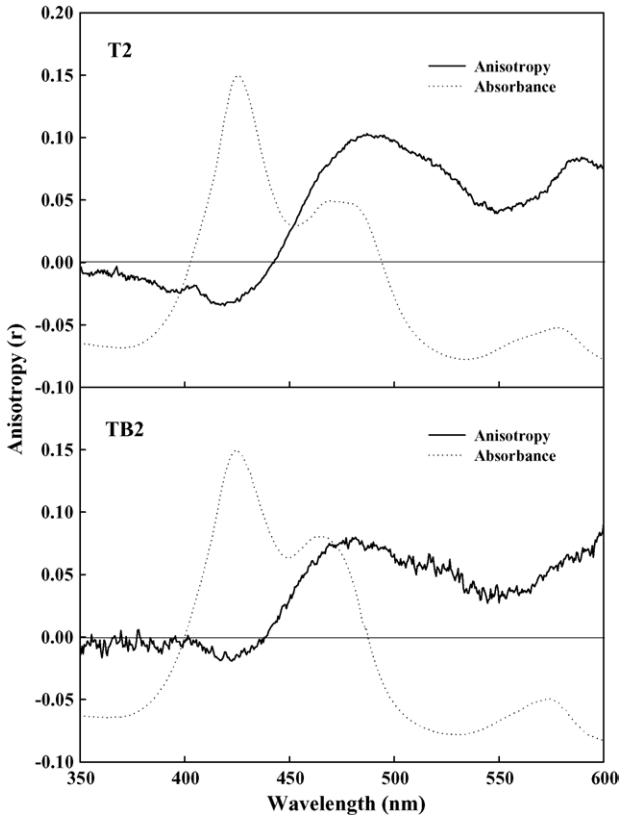


Fig. 2. Steady-state fluorescence excitation anisotropy spectra of **T2** in pyridine and **TB2** in $CHCl_3$. The spectra were obtained with parallel and perpendicular orientations between excitation and emission polarizations, at the fixed emission wavelength 610 nm.

depolarization channel [6,9,14–16]. While **T2** and **TB2** display common anisotropy profiles of *meso–meso* linked zinc(II) porphyrin array, exhibiting negative anisotropy in the high-energy Soret band and positive anisotropies in the low-energy Soret and *Q* bands [6], the absolute anisotropy value over entire absorption spectrum becomes smaller in **TB2**, exhibiting additional depolarization channels presumably because of three-dimensional excitation energy migration over **TB2**.

### *3.3. Fluorescence lifetime and fluorescence anisotropy decay*

The time-resolved fluorescence decays are measured for **T2** and **TB2** (Fig. 3), and their fitted fluorescence lifetimes are

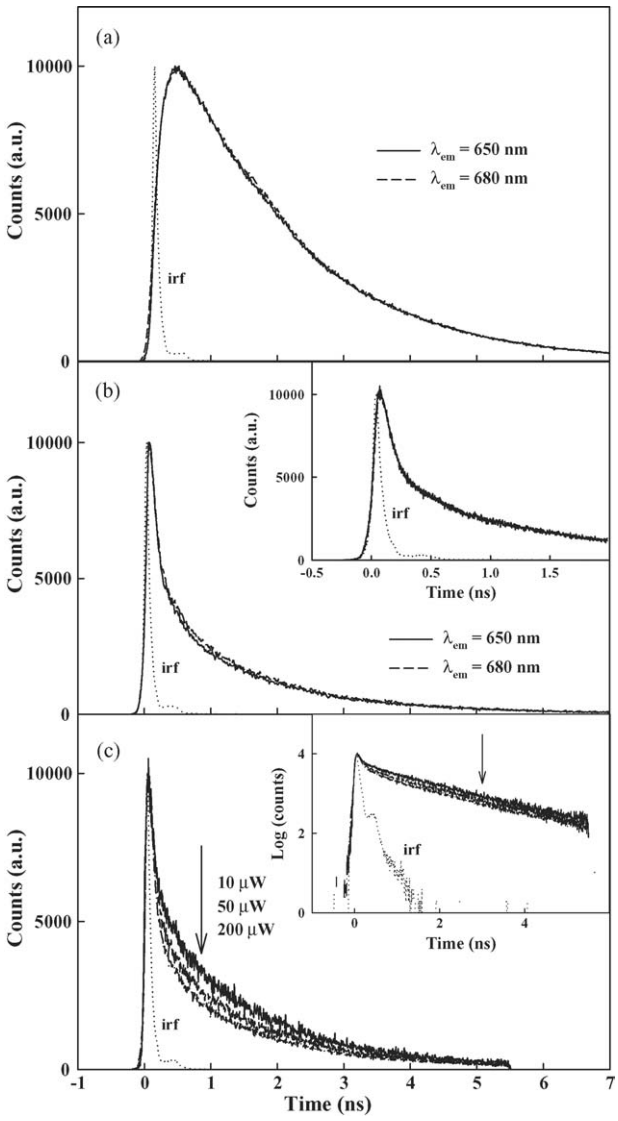


Fig. 3. Time-resolved fluorescence decay profiles of (a) **T2** in pyridine and (b) **TB2** in $CHCl_3$, where the excitation wavelength 420 nm and emission wavelength 650 and 680 nm were used. (c) Excitation power dependent fluorescence decay profiles of **TB2**, of which the excitation wavelength 420 nm and emission wavelength 650 nm were used. IRF represents the instrument response function of the TCSPC system.

Table 2
Fitted fluorescence lifetimes and anisotropy decay parameters of **T2** and **TB2**

| Sample | Fitted fluorescence lifetime (ns)[a] | | | Anisotropy decay time (ns)[b] | |
|---|---|---|---|---|---|
| | $\tau_1$ | $\tau_2$ | $\tau_3$ | $\Phi_1$ | $\Phi_2$ |
| **T2** in pyridine | 1.70 (100%) | | | 1.52 ± 0.03 (−0.074 ± 0.003) | |
| **TB2** in $CHCl_3$ | 0.02 (76%) | 0.18 (16%) | 1.70 (08%) | 7.14 ± 0.80 (−0.038 ± 0.003) | 0.08 ± 0.04 (−0.004 ± 0.002) |

The excitation and emission wavelengths were 420 and 650 nm, respectively.

[a] Using the relation $I(t) = A_1 \exp(-t/\tau_1) + A_2 \exp(-t/\tau_2) + A_3 \exp(-t/\tau_3)$, where $\mathbf{I}(t)$ is the time-dependent fluorescence intensity, $A_i$ the amplitude (noted in parentheses as the normalized percentages i.e. $[A_i/(A_1 + A_2 + A_3)] \times 100$), and $\tau$ the fitted decay time; the $\chi^2$ value of the fittings was maintained as ∼1.0–1.3.

[b] Using the relation $r(t) = r_1 \exp(-t/\Phi_1) + r_2 \exp(-t/\Phi_2)$, where $r(t)$ is the time-dependent fluorescence anisotropy $[r(t) = (I_\parallel(t) - GI_\perp(t))/(I_\parallel(t) + 2G\,I_\perp(t))]$, $r_i$ the initial anisotropy value (noted in parentheses), and $\Phi_i$ the fitted anisotropy decay time.

Table 3
Fluorescence decay parameters of **TB2** depending on excitation power[a]

| Pump power (μW) | Fitted decay times (ps)[b] | | |
|---|---|---|---|
| | $\tau_1$ | $\tau_2$ | $\tau_3$ |
| 10 | 20 (72%) | 180 (15%) | 1700 (13%) |
| 50 | 20 (76%) | 180 (16%) | 1700 (08%) |
| 200 | 20 (77%) | 180 (18%) | 1700 (05%) |

[a] The excitation and emission wavelengths were 420 and 650 nm, respectively.
[b] Using the relation $I(t) = A_1 \exp(-t/\tau_1) + A_2 \exp(-t/\tau_2) + A_3 \exp(-t/\tau_3)$, where $I(t)$ is the time-dependent fluorescence intensity, $A_i$ the amplitude (noted in parentheses as the normalized percentage i.e. $[A_i/(A_1 + A_2 + A_3)] \times 100$), and $\tau$ the fitted decay time. The $\chi^2$ values of the fittings were maintained as ~1.0–1.3.

tabulated (Tables 2 and 3). **T2** shows a single exponential fluorescence decay profile with $\tau_F$ = 1.7 ns, which is similar to that of free **Z3** [6]. In contrast, **TB2** shows a drastic change in fluorescence decay profile (Fig. 2b). The fluorescence exhibits faster decaying profile with time constants of 20, 180, and 1700 ps (Tables 2 and 3), of which fast time constants (20 and 180 ps) are based on the following femtosecond TA measurement with better time-resolution. In order to clarify three decaying components, we examined both emission-wavelength and excitation-power dependences. As a consequence, the fluorescence decay is rather dependent upon the excitation power density than the emission wavelength, in which the faster decaying components (20 and 180 ps) do increasingly contribute to the decay profile as the excitation power increases (Fig. 2c and Table 3). This result implies that the observed three decaying components do not come from multiple fluorescent states but from other deactivation channels in the $S_1$-state of porphyrin. According to our previous report [15] regarding the octameric zinc(II) porphyrin boxes (**B*n***), the pump-power dependence (0.2–1.0 mW) on transient absorption decay was indicative of exciton–exciton annihilation, because the intense excitation or high density of photons generates two or more excitons in one assembling unit, then the recombination between the excitons led to fast deactivation channels. Undoubtedly, the fast fluorescence decaying components occurred in **TB2** are due to exciton–exciton annihilation between the porphyrin units, because of similar architectures. An interest is that the exciton–exciton annihilation occurs with much lower excitation power densities (10–200 μW), compared with the octameric **B*n*** boxes. **B*n*** does not show such faster fluorescence decay profile with a similar excitation power density (~100 μW) [15]. The increased number of chromophores per unit cell is likely to afford a benefit to the exciton–exciton annihilation of **TB2**.

The fluorescence anisotropy decays are measured for **T2** and **TB2**, where the excitation of high-energy Soret band ($\lambda_{ex}$ = 420 nm) was employed (Fig. 4). The fitted decay parameters are tabulated in Table 2. The fluorescence anisotropy decays consistently revealed negative amplitudes in agreement with the negative anisotropies at the high-energy Soret bands of the steady-state excitation anisotropy spectra (Fig. 2). The excitation of the high-energy Soret band is known to induce an incoherent energy hopping within a *meso–meso* linked zinc(II) triporphyrin (**Z3**), which gives rise to a negative fluorescence anisotropy [6]. Because this energy hopping proceeds on the timescale of <200 fs (fourth part of Ref. [6]) it cannot be probed by the TCSPC system. With lower time-resolution in the TCSPC system, we can observe the time constants of rotational diffusion motions of **T2** (1.52 ns) and **TB2** (7.14 ns) (Fig. 4 and Table 2). With highest time-resolution in the TCSPC system, we can also observe a fast anisotropy rising component (~80 ps) in **TB2** that does not occur in **T2** (Fig. 4, insets). This fast rising fluorescence anisotropy indicates the presence of additional depolarization channel reflecting fast excitation energy migration over **TB2**.

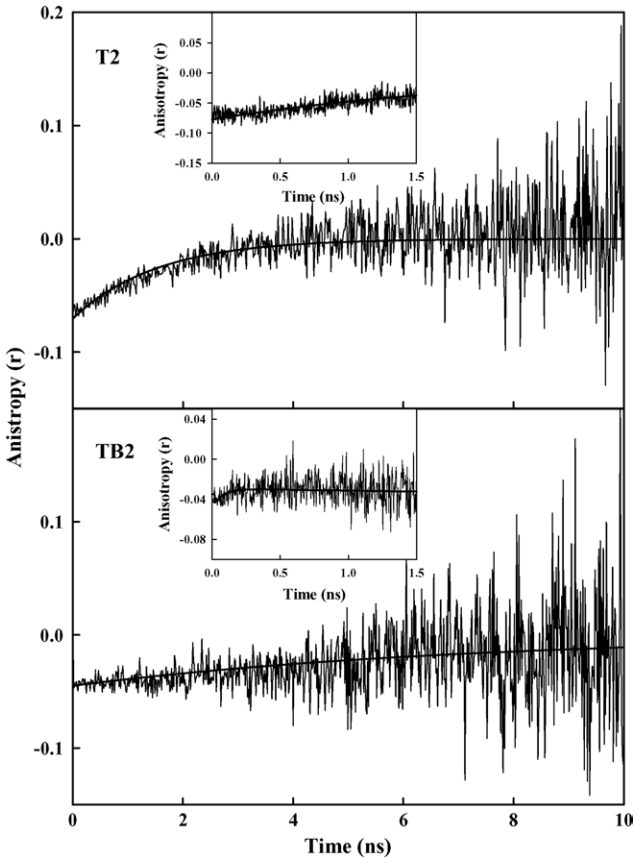


Fig. 4. Time-resolved fluorescence anisotropy decay profiles of **T2** in pyridine and **TB2** in $CHCl_3$. The insets show the decay profiles with better time-resolutions. The excitation wavelength 420 nm and emission wavelength 650 nm were used.

### *3.4. Femtosecond transient absorption (**TA**) and transient absorption anisotropy (**TAA**)*

With much better time resolution of femtosecond TA, we were able to clarify the fast excitation energy migration over **TB2**. Both TA including pump-power dependence and transient absorption anisotropy (TAA) decays of **TB2** are presented (Fig. 5), where the *Q* band excitation ($\lambda_{pump}$ = 570 nm) was employed to avoid the involvement of $S_2$–$S_1$ relaxation [17]. The TA and TAA decays of **T2** are also given as reference (Fig. 5, insets). **T2** reveals slow TA decay in agreement with the $S_1$-state decay (1.7 ns) found in the TCSPC measurement, and concomitantly does not show any anisotropy decay profiles in the time region of hundreds of picoseconds. On the

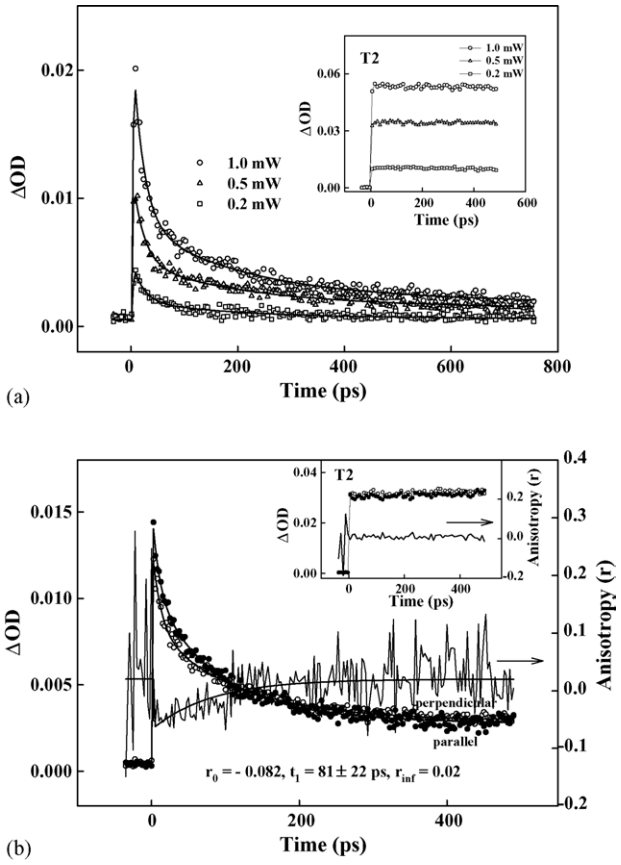


Fig. 5. (a) Transient absorption decay profiles of **TB2** that include pump power dependence. (b) Transient absorption anisotropy decay profiles of **TB2**; the transient absorption decays for parallel and perpendicular orientations between pump and probe polarizations are included, and the fitted decay parameters are inserted. The transient absorption and transient absorption anisotropy decay profiles of **T2** are inserted in the right of each panel. In the experiments, the pump and probe wavelengths are consistently 570 and 510 nm, which are the *Q* band pump and induced absorption probe.

other hand, **TB2** shows relatively fast TA decays along with an anisotropy rise in the same time region, also in agreement with the fluorescence decay measurements in the TCSPC system. The exponential fittings for the TA decays were performed with three decaying components (20, 180, and 1700 ps), in which the slowest time constant (1700 ps) was based on the TCSPC measurement (Table 4). The TA decay is negligibly dependent upon the pump-power (0.2–1.0 mW), which is plausibly understood in terms of pump power saturation to the exciton–exciton annihilation of **TB2**, because of higher excitation powers. In spite of negligible pump power dependence, Fig. 5 indicates that the exciton–exciton annihilation is due to the exciton–exciton recombination between *meso–meso* linked zinc(II) triporphyrins rather than zinc(II) porphyrin monomers, because this process does not occur in **T2**. The TAA decay of **TB2** is fitted with one rising component (81 ps), consistent with the fluorescence anisotropy rising time (80 ps) in the TCSPC measurement (Fig. 5b, inset). Here we note that the TAA shows a single exponential rising component (∼80 ps), even though the TA of **TB2** reveals the two exciton–exciton annihilation components (20 and 180 ps). The discrepancy between the exciton–exciton

Table 4
Transient absorption decay parameters for **T2** and **TB2**[a]

| Pump power (mW) | Fitted decay times (ps)[b] | | |
|---|---|---|---|
| | $\tau_1$ | $\tau_2$ | $\tau_3$ |
| **T2** in pyridine | | | |
| 1.0 | 1700 (100%) | | |
| 0.5 | 1700 (100%) | | |
| 0.2 | 1700 (100%) | | |
| **TB2** in $CHCl_3$ | | | |
| 1.0 | 20 (62%) | 180 (28%) | 1700 (10%) |
| 0.5 | 20 (58%) | 180 (29%) | 1700 (13%) |
| 0.2 | 20 (64%) | 180 (30%) | 1700 (6%) |

[a] The pump and probe wavelengths are 570 and 510 nm, respectively.
[b] Using the relation $\Delta OD(t) = A_1 \exp(-t/\tau_1) + A_2 \exp(-t/\tau_2) + A_3 \exp(-t/\tau_3)$, where $\Delta OD(t)$ is the transient absorption intensity, $A$ the amplitude (noted in parentheses as the normalized percentage i.e. $[A_i/(A_1 + A_2 + A_3)] \times 100$), and $\tau$ the fitted decay time.

annihilation and the anisotropy depolarization, however, has often been found in other multi-chromophoric systems such as LH1 and LH2 systems [18]. In multi-chromophoric system, neither exciton–exciton annihilation nor anisotropy depolarization time is directly ascribed to the excitation energy hopping time, because they do not occur in simple donor–acceptor pair. The energy hopping time can only be theoretically obtained by modeling the process (vide infra).

## 4. Discussion

Similar to other free *meso–meso* linked zinc(II) triporphyrin (**Z3**)s, **T2** shows split Soret bands due to exciton coupling. The Soret band of zinc(II) porphyrin monomer has two perpendicular transition dipole moments; $B_x$ and $B_y$ that are degenerate in a simple monomer (Scheme 2, left). In a *meso–meso* linked zinc(II) triporphyrin, however, parallel three $B_z$s couple effectively, whereas other dipole interactions should be virtually zero because of an averaged perpendicular conformation (Scheme 2, middle). The Soret bands of **T2** consequently are split into a red-shifted $B_z$ component and unperturbed $B_x$ and $B_y$ components.

It is interesting to note that the box **TB2** exhibits a smaller Soret band splitting energy than those of **T2** and **Z3**. We interpret this result in terms of three-dimensional exciton coupling scheme as described below. Even though the Soret band splitting of **T2** is explained by simple excitonic dipole coupling between zinc(II) porphyrin monomers [6], more complicated Soret band splittings are expected in **TB2**, because various dipole–dipole excitonic interactions are possible among 12 mutually perpendicular porphyrin units (Scheme 2, right). As a result of 24 possible exciton coupling states of **TB2**, split Soret bands are clearly observable (Fig. 1 and Table 1). The low-energy Soret state indicates excitonic dipole–dipole interaction among 12 parallel transition dipole moments along the *z*-axis, whereas the high-energy Soret state implies excitonic dipole–dipole interaction among six parallel transition dipole moments along the *x*- or *y*-axis. In order to calculate the band splitting energy of **TB2** in comparison with that of **T2**, we attempt to diagonalize the matrix whose elements are the coupling energies ($V_{ij}$). In **TB2**,

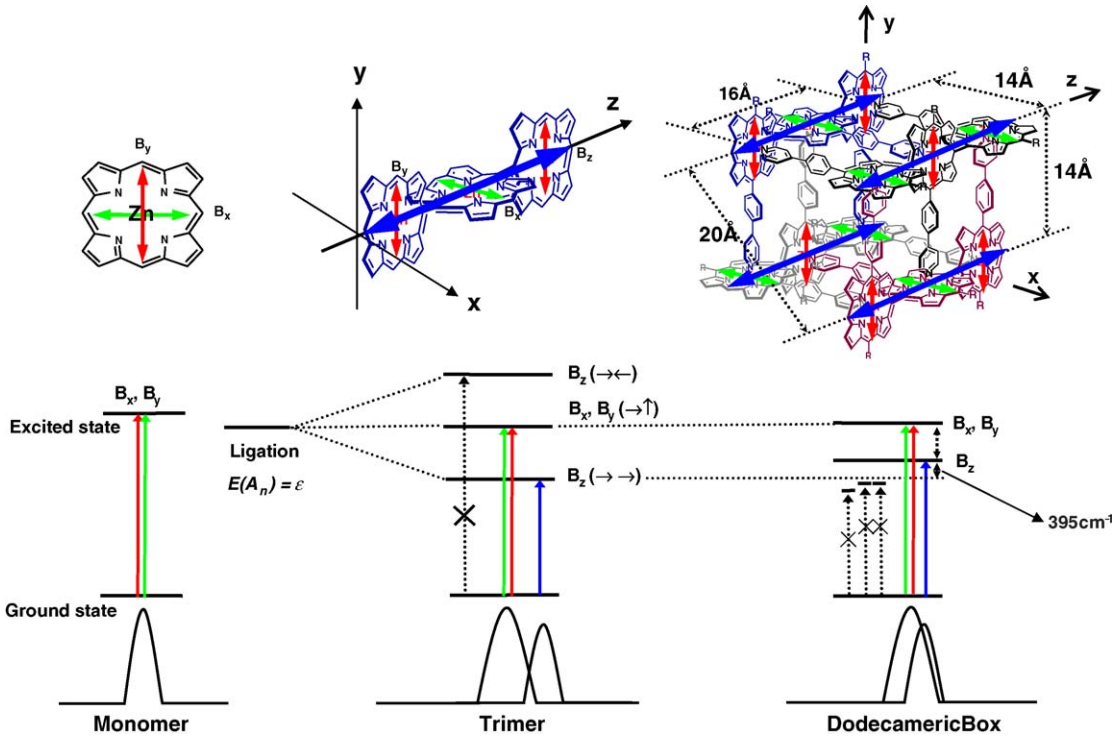


Scheme 2. Exciton coupling in porphyrin monomer, *meso–meso* linked triporphyrin, and dodecameric porphyrin box.

assuming that the dipoles in the $z$-axis among three porphyrin monomer units in the constituent porphyrin trimer for the box formation are strongly interacting to form one coherently coupled state, we can obtain four possible coupling energies among them (Scheme 2) [19].

The dipole coupling energy, $V_{ij}$, can be calculated as [20]:

$$V_{ij} = \frac{5.04 f_L^2 |\vec{\mu}| |\vec{\mu}_{ij}| \kappa_{ij}}{\varepsilon_{op} R_{TS}^3} \quad (1)$$

where $\varepsilon_{op}$ is the dielectric constant at optical frequencies, $f_L$ the Lorentz local field correction factor, $f_L = (\varepsilon_{op} + 2)/3$, and $\kappa_{ij}$ the orientation factor [21] of the two dipoles $|\vec{\mu}_i|$ and $|\vec{\mu}_j|$, and $R_{TS}$ the through-space center-to-center distance. In this equation, the coupling energy is expressed in $cm^{-1}$, the transition dipoles in Debye and the distance in nm. Then, $V_{ij}$ can be expressed in the form of $4 \times 4$ matrix:

$$V_{ij} = \begin{pmatrix} 0 & 168 & 59 & 168 \\ 168 & 0 & 168 & 59 \\ 59 & 168 & 0 & 168 \\ 168 & 59 & 168 & 0 \end{pmatrix} \quad (2)$$

where $i, j = 1, 2, 3, 4$.

The $\varepsilon_{op}$ is 9.1 for $CH_2Cl_2$ at room temperature, and the orientation factor $\kappa_{ij}$ is 1. Upon the diagonalization of the interacting matrix, the resulting four excitonic coupled energy states compared to noninteracting case are obtained as four eigenvalues; $-277$, $-59$, $-59$, $395\ cm^{-1}$. As the magnitudes of all four transition dipoles are the same and the eigenvectors corresponding to the eigenvalues are the relative contribution for each transition dipole, only the upper excitonic state $\Delta E = 395\ cm^{-1}$ due to the coupling of the $B_z$ dipoles is optically accessible, showing the blue shift of low-energy Soret band with respect to the initial position of non-interacting low-energy Soret band. The other three eigenvalues indicate dark states, that is, the vector summation of interacting dipoles are equal to 0, and their excitonic states cannot be populated upon absorption of light. As a result, according to the B band splitting energy of monomer ($2400\ cm^{-1}$) in Table 1, that of **TB2** can be calculated to be $\Delta E = 2005\ cm^{-1}$ ($2005 = 2400–395\ cm^{-1}$), which is in a good agreement with the experimental values, $\Delta E = 2000\ cm^{-1}$ [22].

The exciton–exciton annihilation that depends upon laser power has provided rich information about the excitation energy migrations within the natural light-harvesting antenna of LH1 and LH2, in which the exciton–exciton annihilation was understood in terms of formation of a doubly excited state as a consequence of Förster-type incoherent energy transfer upon the absorption of more than two photons in a single molecular entity. The doubly excited state thus formed quickly relaxes to the singly excited state [17,18]. Consequently, the observed exciton–exciton annihilation is a direct evidence of the Förster-type incoherent energy hopping among many orthogonally associated zinc(II) triporphyrins of **TB2**. It is noteworthy that the two fast annihilation components ($\tau_1 = 20$ ps and $\tau_2 = 180$ ps) are observed in **TB2**. However, it is usually known that the energy hopping process is a migration-limited process rather than a trapping-limited process, and the slowest exciton–exciton annihilation component can describe the Förster-type incoherent energy hopping over entire architecture [17,18].

We have examined the excitation energy migration of **TB2** using the exciton–exciton annihilation and anisotropy depolarization. Here we quantify the energy hopping time with these two observables. The description of the exciton–exciton annihilation and anisotropy depolarization has been well developed for LH1 and LH2 that have cyclic multi-porphyrin architectures [17,18]. In LH1 and LH2, an explicit Förster-type incoherent energy hopping model has been constructed assuming a migration-limited character of exciton–exciton annihilation, and a random walk formalism of anisotropy. In this context, the analytical depolarization and exciton–exciton annihilation times are connected with the excitation energy hopping time by the following equations [17],

$$\tau_{\text{depolarization}} = \frac{\tau_{\text{hopping}}}{4(1-\cos^2(2\pi/N))} = \frac{\tau_{\text{hopping}}}{4(1-\cos^2\alpha)} \quad (3)$$

$$\tau_{\text{annihilation}} = \frac{N^2-1}{24}\tau_{\text{hopping}} \quad (4)$$

where $N$ is the number of hopping sites and $\alpha$ the angle between adjacent transition dipoles. The number of hopping sites $N$ is defined by $N_m/L$, where $N_m$ is the number of molecules and $L$ the exciton coherence length of the array [18]. The $\tau_{\text{annihilation}}$ value in Eq. (4) is also defined as the slowest exciton–exciton annihilation time that reflects a migration-limited character of the exciton [23]. Eq. (3) is understood by considering that the depolarization is complete when the transition dipole migrates through 90° and by considering how many hops are required for this rotation to be accomplished. On the other hand, Eq. (4) assumes that the exciton–exciton annihilation reflects the migration limited exciton–exciton recombination process along the whole cyclic array and how many hops are required for this recombination to be accomplished.

**TB2** has 12 mutually perpendicular porphyrin units, however, the number of hopping sites is $N = 4$, because the hopping units are four *meso–meso* linked zinc(II) triporphyrins that have the exciton coherence length of $L = 3$, respectively. Although the exciton coherence length of the orthogonally linked zinc(II) porphyrin array is known to be $L = 4$–5 in the $Q$ state [6], the exciton coherence length of **TB2** is $L = 3$, because of its noncovalent linkages. In order to describe the random walk of the anisotropy, the orientations of the molecular transition dipoles should be considered. As shown in Scheme 2, right, the transition dipoles that are attributable to the change of anisotropy are arranged in a square cycle on *xy*-plane; the energy hopping among the transition dipoles along *z*-axis does not change the anisotropy. Consequently, the anisotropy decay profile of **TB2** reflects the energy hopping process occurring in square *xy*-plane that consists of mutually perpendicular four transition dipole moments. This consideration makes **TB2** a cyclic porphyrin array and concomitantly Eqs. (3) and (4) are used. Introducing $\alpha = 90°$ and $N = 4$, the relations $\tau_{\text{hopping}} = 4 \times \tau_{\text{depolarization}}$ and $\tau_{\text{hopping}} = 1.6 \times \tau_{\text{annihilation}}$ are obtained for **TB2**. The energy hopping time accordingly is calculated to be 324 ps with the anisotropy rise time (81 ps) given in Fig. 5. In a different approach, the energy hopping time is also estimated to be 288 ps with the slowest exciton–exciton annihilation component ($\tau_2 = 180$ ps) listed in Table 3. It is interesting that the two different observables, exciton–exciton annihilation and anisotropy depolarization, result in a consistent excitation energy hopping time with a small error ($300 \pm 20$ ps). The excitation energy migration over **TB2** consequently is well described by the Förster-type incoherent energy hopping model, plausibly because of their rigid and well-defined perpendicaulr orientations. Another interest is that **TB2** reveals slower energy hopping time ($300 \pm 20$ ps) than the previous $98 \pm 3$ ps of **B2** (an octameric porphyrin box), even though they have the same intercoordination distance (14 Å) between the hopping units (di- or tri-porphyrin). This observation indicates that the energy hopping time becomes slower as the size of hopping unit increases from two to three zinc(II) porphyrins. The energy hopping time consequently reflects intra-energy equilibrium process within the hopping site, which is slower in longer zinc(II) triporphyrin. From a viewpoint of light harvesting, more choromopores per unit cell, however, have a benefit in terms of light absorbing ability. Consequently, two counteracting properties, i.e., the hopping time and the size of hopping unit should be in an effective ensemble to give the highest light harvesting efficiency, such as diporphyrin hopping unit in the natural LH2 antennae.

## 5. Conclusions

One of the key requirements for molecular design of photosynthetic modules is a precise control of electronic interaction between porphyrin-like chromophores, since the electronic interaction is a key parameter in determining excitation energy transfer and electron transfer. This control is often very difficult in noncovalent assemblies, because of low chemical stability and ambiguous spatial arrangement. This stands in a sharp contrast to strictly arranged chromophore arrays in the natural antenna systems. Zinc(II) insertion into meso-pyridyl-appended *meso–meso* linked triporphyrin (**T2**)s drives the formation of dodecameric porphyrin box (**TB2**). Interestingly, the box formation is accompanied by rigidification of the perpendicular conformation of *meso–meso* linked triporphyrin, leading to very precise fixation of the spatial arrangement and hence the electronic coupling among porphyrins, which allow for various steady-state and ultrafast measurements. The high- and low-energy Soret bands of **TB2** are indicative of excitonic dipole–dipole interactions among six parallel transition dipole moments along the *x* or *y* axis and among 12 parallel transition dipole moments along the *z*-axis, respectively, which consequently bring about an energy migration over three-dimensional space. The relatively small polarization anisotropy observed in the steady-state fluorescence excitation spectra reflect the efficient excitation energy migration over **TB2**. The exciton–exciton annihilation and the anisotropy rise observed in both time-resolved fluorescence and femtosecond transient absorption describe well the excitation energy hopping rate over **TB2**. Modeling of the energy migration process within **TB2** with $N = 4$ and $L = 3$ consistently give the excitation energy hopping time of $300 \pm 20$ ps among the *meso–meso* linked zinc(II) triporphhyrins, which is slower than the previous $98 \pm 3$ ps of **B2** (an octameric zinc(II) porphyrin box). After all, the excitation energy migration of **TB2** is well

described by the Förster-type incoherent energy-hopping model, because of its well-defined perpendicular orientations. In addition, the energy hopping time reflects intra-energy equilibrium process within the hopping site, which becomes slower in longer zinc(II) triporphyrin of **TB2**.

## Acknowledgments

The work at Yonsei was financially supported by the National Creative Research Initiatives Program of the Ministry of Science and Technology of Korea to D. Kim. The work at Kyoto was partly supported by Grant-in-Aid from the Ministry of Education, Culture, Sports, Science and Technology, Japan and 21st Century COE on Kyoto University Alliance for Chemistry to A. Osuka. The authors greatly thank Prof. Eric Vauthey (University of Geneva, Genève, Switzerland) for his kind comments.

## References

[1] M.R. Wasielewski, Chem. Rev. 92 (1992) 435.
[2] D. Gust, T.A. Moore, A.L. Moore, Acc. Chem. Res. 34 (2001) 40.
[3] D. Holten, D.F. Bocian, J.S. Lindsey, Acc. Chem. Res. 35 (2002) 57.
[4] M.P. Debreczeny, W.A. Svec, E.M. Marsh, M.R. Wasielewski, J. Am. Chem. Soc. 118 (1996) 8174.
[5] G. Kodis, P.A. Liddell, L. de la Garza, P.C. Clausen, J.S. Lindsey, A.L. Moore, T.A. Moore, D. Gust, J. Phys. Chem. A 106 (2002) 2036.
[6] D. Kim, A. Osuka, Acc. Chem. Res. 37 (2004) 735, and references are therein;
D. Kim, A. Osuka, J. Phys. Chem. A 107 (2003) 8791, and references are therein;
Y.H. Kim, D.H. Jeong, D. Kim, S.C. Jeoung, H.S. Cho, S.K. Kim, N. Aratani, A. Osuka, J. Am. Chem. Soc. 123 (2001) 76;
H.S. Cho, N.W. Song, Y.H. Kim, S.C. Jeoung, S. Hahn, D. Kim, S.K. Kim, N. Yoshida, A. Osuka, J. Phys. Chem. A 104 (2000) 3287;
N. Aratani, A. Osuka, Y.H. Kim, D.H. Jeong, D. Kim, Angew. Chem. Int. Ed. 39 (2000) 1458;
Y.H. Kim, H.S. Cho, D. Kim, S.K. Kim, N. Yoshida, A. Osuka, Syn. Met. 117 (2001) 183;
N. Aratani, A. Osuka, H.S. Cho, D. Kim, J. Photochem. Photobiol. C: Photochem. Rev. 3 (2002) 25;
C.-K. Min, T. Joo, M.-C. Yoon, C.M. Kim, Y.N. Hwang, D. Kim, N. Aratani, N. Yoshida, A. Osuka, J. Chem. Phys. 114 (2001) 6750;
H.S. Cho, D.H. Jeong, M.-C. Yoon, Y.-R. Kim, D. Kim, S.C. Jeoung, S.K. Kim, N. Aratani, H. Shinmori, A. Osuka, J. Phys. Chem. A 105 (2001) 4200;
D.H. Jeong, M.-C. Yoon, S.M. Jang, D. Kim, D.W. Cho, N. Yoshida, N. Aratani, A. Osuka, J. Phys. Chem. A 106 (2002) 2359;
N. Aratani, H.S. Cho, T.K. Ahn, S. Cho, D. Kim, H. Sumi, A. Osuka, J. Am. Chem. Soc. 125 (2003) 9668;
M.-C. Yoon, J.K. Song, S. Cho, D. Kim, Bull. Kor. Chem. Soc. 24 (2003) 1075;
N.W. Song, H.S. Cho, M.-C. Yoon, S.C. Jeoung, N. Yoshida, A. Osuka, D. Kim, Bull. Kor. Chem. Soc. 75 (2002) 1023;
I.-W. Hwang, N. Aratani, A. Osuka, D. Kim, Bull. Kor. Chem. Soc. 26 (2005) 19.
[7] N. Yoshida, D.H. Jeong, H.S. Cho, D. Kim, Y. Matsuzaki, K. Tanaka, A. Osuka, A. Chem. Eur. J. 9 (2003) 58;
D.H. Jeong, S.M. Jang, I.-W. Hwang, D. Kim, N. Yoshida, A. Osuka, J. Phys. Chem. A 106 (2002) 11054;
H.S. Cho, J.K. Song, J.-H. Ha, S. Cho, D. Kim, N. Yoshida, A. Osuka, J. Phys. Chem. A 107 (2003) 1897;
H. Shinmori, T.K. Ahn, H.S. Cho, D. Kim, N. Yoshida, A. Osuka, Angew. Chem. Int. Ed. 42 (2003) 2754.
[8] A. Tsuda, A. Osuka, Science 293 (2001) 79;
H.S. Cho, D.H. Jeong, S. Cho, D. Kim, Y. Matsuzaki, K. Tanaka, A. Tsuda, A. Osuka, J. Am. Chem. Soc. 124 (2002) 14642;
D.H. Jeong, S.M. Jang, I.-W. Hwang, D. Kim, Y. Matsuzaki, K. Tanaka, A. Tsuda, T. Nakamura, A. Osuka, J. Chem. Phys. 119 (2003) 5237.
[9] X. Peng, N. Aratani, A. Takagi, T. Matsumoto, T. Kawai, I.-W. Hwang, T.K. Ahn, D. Kim, A. Osuka, J. Am. Chem. Soc. 126 (2004) 4468;
Y. Nakamura, I.-W. Hwang, N. Aratani, T.K. Ahn, D.M. Ko, A. Takagi, T. Kawai, T. Matsumoto, D. Kim, A. Osuka, J. Am. Chem. Soc. 127 (2005) 236;
I.-W. Hwang, D.M. Ko, T.K. Ahn, Z.S. Yoon, D. Kim, X. Peng, N. Aratani, A. Osuka, J. Phys. Chem. 109 (2005) 8643.
[10] J.-M. Lehn, Science 295 (2002) 2400;
M.D. Hollingsworth, Science 295 (2002) 2410.
[11] C.A. Hunter, J.K.M. Sanders, G.S. Beddard, S. Evans, J. Chem. Soc., Chem. Commun. (1989) 1765;
S. Anderson, H.L. Anderson, J.K.M. Sanders, Acc. Chem. Res. 26 (1993) 469.
[12] G.S. Wilson, H.L. Anderson, Chem. Commun. (1999) 1539;
P.N. Taylor, H.L. Anderson, J. Am. Chem. Soc. 121 (1999) 11538;
T.E. Screen, J.R.G. Thorne, R.G. Denning, D.G. Bucknall, H.L. Anderson, J. Am. Chem. Soc. 124 (2002) 9712;
T.E. Screen, J.R.G. Thorne, R.G. Denning, D.G. Bucknall, H.L. Anderson, J. Mater. Chem. 12 (2003) 2796.
[13] C.A. Hunter, R.K. Hyde, Angew. Chem., Int. Ed. Engl. 35 (1996) 1936;
R.A. Haycock, A. Yartsev, U. Michelsen, V. Sundström, C.A. Hunter, Angew. Chem. Int. Ed. 39 (2000) 3616.
[14] K. Ogawa, Y. Kobuke, Angew. Chem. Int. Ed. 39 (2000) 4070;
K. Ogawa, T. Zhang, K. Yoshihara, Y. Kobuke, J. Am. Chem. Soc. 124 (2002) 22;
R. Takahashi, Y. Kobuke, J. Am. Chem. Soc. 125 (2003) 2372;
I.-W. Hwang, M. Park, T.K. Ahn, Z.S. Yoon, D.M. Ko, D. Kim, F. Ito, Y. Ishibashi, S.R. Khan, Y. Nagasawa, H. Miyasaka, C. Ikeda, R. Takahashi, K. Ogawa, A. Satake, Y. Kobuke, Chem. Eur. J. 11 (2005) 3753.
[15] I.-W. Hwang, T. Kamada, T.K. Ahn, D.M. Ko, T. Nakamura, A. Tsuda, A. Osuka, D. Kim, J. Am. Chem. Soc. 126 (2004) 16187;
I.-W. Hwang, H.S. Cho, D.H. Jeong, D. Kim, A. Tsuda, T. Nakamura, A. Osuka, J. Phys. Chem. B 107 (2003) 9977;
A. Tsuda, T. Nakamura, S. Sakamoto, K. Yamaguchi, A. Osuka, Angew. Chem. Int. Ed. 41 (2002) 2817.
[16] M.M. Yatskou, R.B.M. Koehorst, A. van Hoek, H. Donker, T.J. Schaafsma, B. Gobets, I. van Stokkum, R. van Grondelle, J. Phys. Chem. A 105 (2001) 11432;
M.M. Yatskou, H. Donker, E.G. Novikov, R.B.M. Koehorst, A. van Hoek, V.V. Apanasovich, T.J. Schaafsma, J. Phys. Chem. A 105 (2001) 9498.
[17] S.E. Bradforth, R. Jimenez, F. van Mourik, R. van Grondelle, G.R. Fleming, J. Phys. Chem. 99 (1995) 16179.
[18] G. Trinkunas, J.L. Herek, T. Polívka, V. Sundström, T. Pullerits, Phys. Rev. Lett. 86 (2001) 4167;
G. Trinkunas, J. Luminesc. 102 (2003) 532;
B. Brüggemann, V. May, J. Chem. Phys. 120 (2004) 2325;
M.G. Müller, M. Hucke, M. Reus, A.R. Holzwarth, J. Phys. Chem. 100 (1996) 9537;
B. Brüggemann, J.L. Herek, V. Sundström, T. Pullerits, V. May, J. Phys. Chem. B 105 (2001) 11391.
[19] A. Morandeira, E. Vauthey, A. Schuwey, A. Gossauer, J. Phys. Chem. A 108 (2004) 5741.
[20] H. van Amerongen, L. Valcunas, R. van Grondelle, Photosynthetic Excitons, World Scientific, Singapore, 2000.
[21] J. Michl, E.W. Thulstrup, Spectroscopy with Polarized Light, VCH, 1986.
[22] The dipole coupling energies of $x$ and $y$ axis can be calculated by diagonalization as the following eigenvalues; −44, −85, −139, −269, 93, 444, six zeros $cm^{-1}$. Among these, only −85, −139, and six zeros can be determined to be dark states (−85, −139) or noninteracting (six zeros), but the other four eigenvalues, −44, −269, 93, 444 can-

not be determined to be either allowed or forbidden transition due to the complicated eigenvectors in the analysis of the eigenvalues. However, according to the absorption spectrum, the interaction among the transition dipoles of $x$ or $y$ axis is estimated to be apparently small. As a result, regardless of the allowed or forbidden transition of interacting $x$ and $y$ axis', the dipole coupling energies in $x$ and $y$ axis' are small enough to be ignored, because the excitonic state formed by transition dipole coupling in $x$ and $y$ axis' cannot be observed in UV absorption spectrum or calculated by diagonalization of interacting matrices.

[23] M.M. Yatskou, R.B.M. Koehorst, H. Donker, T.J. Schaafsma, J. Phys. Chem. A 105 (2001) 11425.